UNIVERSAL WISER
PUBLISHER

Research Article

A Comparison of Predicted Distortion of a Manifold Fabricated by Laser Powder Bed Fusion Using Solid and Shell Element-based Finite Element Models

Hafizur Rahman[1], Kamen Uzunov[2] (ID), Shukri Afazov[1]* (ID)

[1]Department of Engineering, Nottingham Trent University, Nottingham, NG11 8NS, United Kingdom
[2]Department of Industrial Design, University of Ruse, Ruse, Bulgaria
 E-mail: shukri.afazov@ntu.ac.uk

Abstract: This paper compares the predicted distortion of a manifold geometry fabricated by laser powder bed fusion between an established finite element model using solid elements and a newly developed in this paper finite element model using shell elements. The developed finite element models utilized two methods to induce a strain field (inherent strain and analytical thermal methods). The predicted distortions from these models were also compared with experimentally measured distortions. The results showed that the predicted distortion using solid elements is more suitable to predict the buckling effect on the manifold geometry. Despite that, the model using shell elements showed an accurate prediction of distortion in many areas of the manifold, and it proved to be computationally more efficient (2.4 times faster), this model showed lower accuracy in the prediction of distortion generated by buckling. However, shell elements could be used in other applications where the bucking is not the driving mechanism for the prediction of distortion in laser powder bed fusion or in applications where the accuracy of distortion is not a requirement (e.g., support structures).

Keywords: additive manufacturing, finite element analyses, shell elements, distortion

1. Introduction

Additive manufacturing (AM) gained large attention in the last decade [1]. Despite the advantages in geometry versatility and waste mitigation, products made by AM technology could experience undesirable internal defects and residual stresses causing dimensional inaccuracy due to distortion. The recent developments in laser powder bed fusion (LPBF) gained momentum for the manufacturing of industrial components [2]. One of the key considerations in LPBF is the residual stresses that cause distortions in the components [3]. The cause of residual stress and distortion on geometries produced by LPBF is due to abrupt thermal gradients that create a non-uniform plastic flow due to phase transformations during cooling [4]. During the phase transformation, a volumetric change occurs causing an increased thermal expansion. This volume difference results in material contraction or expansion causing the generation of residual stress. The ability to predict the residual stresses and distortion in LPBF can aid the product development of industrial components [5].

The finite element method was widely used for the prediction of distortion in LPBF [6]. One of the methods

that was used to predict residual stresses and distortion in AM is the inherent strain method (ISM), which was widely adopted in commercial software tools [7]. A key advantage of the ISM is the ability to reduce the complexity of the thermo-mechanical simulation to a purely mechanical problem, which can lead to a decrease in simulation processing time [8]. Although the ISM has greater computational performance, the method is not capable of simulating the effect of the machine settings (hatch distance, power, speed and powder characteristics and distribution during raking). Lindgren [9] conducted experimentation on a weld model subjected to thermal strains that were successfully used to study buckling effects and distortion. Gysin et al. [10] found a strong correlation between predicted and measured distortion for a wide range of geometries using the ISM with solid elements. Liang et al. [11] modified the ISM in metal AM components by considering a large temperature gradient to increase the accuracy of the method. Afazov et al. [12] developed a method using an analytical temperature field to induce thermal strains to predict residual stresses and distortion for a thin Ti6Al4V structure and a stainless steel 17-4PH turbine blade. Later, Afazov et al. [13] demonstrated a comparison of the ISM and the analytical temperature field of an industrial impeller made of Inconel 718 using solid elements. The results showed that the ISM using the elastoplastic material model delivered the best correlation with experimental measurements of distortion. In welding, the ISM was used to reduce computational time in simulations of large structures using shell elements, where the inherent strains were applied in one step [14]. However, the layer-by-layer activation of elements and applying inherent strain values require multiple steps in the simulation of the LPBF build process.

Despite the conducted research in the simulation of the LPBF build process, the combination of the layer-by-layer activation of shell elements and the use of the ISM has not been addressed in the simulation of the LPBF build process. Therefore, the main objective of this research is to develop novel finite element models using shell elements for the first time that are capable of predicting the distortion of a manifold geometry fabricated by LPBF as well as to compare the results with experimental measurements and predicted distortion using solid elements from [15]. Another objective is to analyze the computational time and understand the computational gain of the shell elements. The paper first presents the developed finite element models followed by the comparison of the results and concluding the key findings.

2. Methodology

2.1 Overview of experimental procedures

A manifold structure with a height of 210 mm and a thickness of 1.5 mm is used in this study. The manifold was manufactured using the EOS M290 LPBF machine and optically scanned as described in [15]. The material was Inconel 718. The manifold was manufactured in an argon atmosphere by applying a laser power of 190 W, a laser scanning velocity of 800 mm/s, a layer thickness of 40 μm, a hatching distance of 90 μm and a stripe scanning strategy. The preheating temperature of 100 °C was also applied to the build plate as well as a 10 s dwell time between two successive deposited layers. There was no post-heat treatment applied to the build plate and the manifold. The manufactured manifold is shown in Figure 1.

Figure 1. LPBF built of a thin Inconel 718 manifold

2.2 *Finite element shell model*

In this study, the manifold geometry was converted from a solid into a surface model in ANSYS. The surface model was sliced into layers with a layer size of 1 mm. After slicing, a mesh with shell elements was generated. The mesh consisted of 30,729 nodes and 10,233 8-node quadratic shell elements. A thickness of 1.5 mm was assigned to the tube section of the manifold (see Figure 1), while a thickness of 5.5 mm was assigned to the base section to represent the actual geometry. Figure 2 shows the mesh of the manifold geometry as well as the sliced layers.

Figure 2. Mesh of the manifold model with shell elements (note that the shell thickness is displayed)

The element birth technique was used to activate the elements using the layer-by-layer technique [16]. In the finite element theory, all elements of the geometry are allocated in a stiffness matrix. The activated elements have a stiffness while the deactivated elements, known as non-active, are represented with a null stiffness ("dummy elements"). Once the non-active elements are activated, the material properties for those activated layers are changed from null to the assigned material data, known as "birth".

2.3 *Implementation of the ISM*

Figure 3 illustrates how the inherent strain approach is incorporated into the formulations of the finite element

method. The corresponding functions ε^*, ε, ε^e, f, u, and σ represent the vector components for the inherent strain, total strain, elastic strain, equivalent nodal load, nodal displacement and stress, respectively. The vector components are accompanied by matrix functions of the inherent strain where $[B]$, $[D]$, and $[K]$ are terms for the strain-displacement, elastic-strain and stiffness matrix, respectively [16].
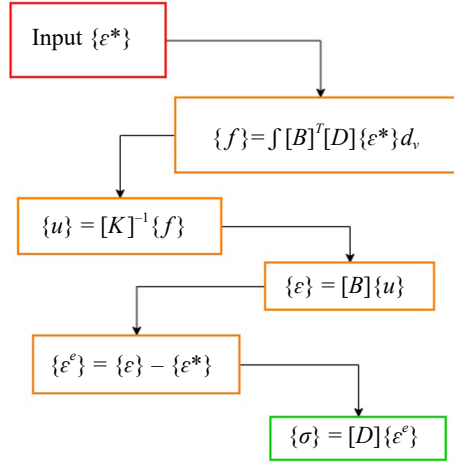
Figure 3. Finite element formulations with integrated inherent ISM

The ISM was implemented in ANSYS by prescribing a temperature in the elements. A temperature was changed from 0 to 1 degree and the inherent strain value was prescribed as a coefficient of thermal expansion. The following material properties were used: Young's modulus of 170 GPa, the yield stress of 620 MPa and a coefficient of thermal expansion of -0.0037 C^{-1}. At a temperature change of 1 °C, the applied coefficient of thermal expansion will induce a compressive strain of -0.0037 in the activated elements in all three directions (x, y and z). Static structural analyses with a material model with perfect plasticity were conducted.

2.4 Implementation of the analytical thermal method

Afazov et al. [12] developed a method using an analytical temperature field across the component to induce thermal strains, which was adopted in this study to understand its accuracy in thin-walled structures. The applied thermal strain for the analytical temperature field is provided by $\{\varepsilon'\} = \alpha\{\Delta T\}$, where α is the coefficient of thermal expansion and ΔT is the temperature change. The temperature change in the build direction can be calculated by:

$$\{\Delta T\} = \frac{2Q}{C\rho(4\pi at)^{1.5}}\left(e^{-\frac{(\{Z\}-\{Z'_i\})^2}{4at}} - e^{-\frac{(\{Z\}-\{Z'_{i-1}\})^2}{4at}}\right) \tag{1}$$

where Q, C, ρ, a, and t represent the power distribution, specific heat capacity, density, thermal diffusivity and time, respectively. Z is the coordinate in the vertical direction of the finite model, Z'_i is the coordinate in the vertical direction of the activated field in the i layer, and finally, Z'_{i-1} is the coordinate in the vertical direction of the previously activated layer i-1.

The analytical temperature field method was implemented in ANSYS by prescribing a temperature in the elements using Eq. 1 via APDL commands. Temperature-dependent Young's modulus, yield stress and coefficient of thermal expansion (see Table 1) were used in static structural analyses using a material model with perfect plasticity.

Table 1. Temperature dependent material properties for Inconel 718

Temperature (°C)	Young's Modulus (GPa)	Yield Stress (MPa)	Coefficient of Thermal Expansion (°C⁻¹)
20	170	720	1.37E-05
300	167	618	1.44E-05
600	149	562	1.74E-05
800	138	530	1.99E-05
900	111	268	2.10E-05
1000	79	81	2.16E-05

3. Results and discussion

The simulation time for the model with solid elements from [15] was approximately 6 hours while the shell model using ISM was solved in 2.5 hours. Both simulations were run on an Intel(R) Core™ i5-4200U using 2 cores. The shell model with the analytical thermal solution was completed in 3.5 hours. The computational time was greater due to the fact that this method solved temperature-dependent mechanical properties leading to greater non-linearities. A material deposition in four stages of the build process is shown in Figure 4. It needs to be noted that a deformation scale factor of 30 was applied to better visualize the deformation behaviour during the build process. It can be seen that the stress distribution changes by activating more layers, which is expected due to the change in the overall stiffness. Compared to the original undeformed shape, it can be seen that the simulated manifold tends to shrink.

	664.73		543.87		423.01		302.15		181.29		60.43	
725.17		604.3		483.44		362.58		241.72		120.86		0
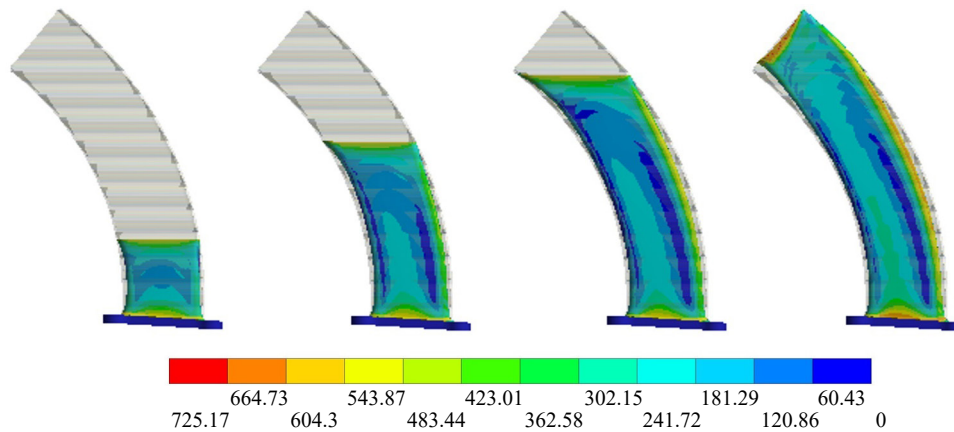
Figure 4. Simulation of the LPBD build process using the ISM (shell model), units in MPa

Figure 5a shows the surface deviations calculated between the experimentally measured data points using optically scanning and the original CAD geometry [15]. The surface deviations were calculated in the GOM Inspect software after the two geometries were first aligned. The surface deviations are used to benchmark the results generated by the models in this study. Figures 5b-d show the surface deviations calculated from the distorted geometry from the models to the original CAD geometry for the solid model using the ISM, shell model using the ISM and shell model using the analytical temperature field, respectively. By comparing the three models to the experimental results, it can be seen that the solid model using the ISM shows the best correlation of surface deviations. The shell model using the ISM shows lower surface deviations in general. Key areas where the shell model using the ISM delivered better correlation with

experimental results is at the edge boundary for the outer and inner edges (see Figures 6 and 7). It can be seen that the surface deviations at the inner and outer edges of the shell model using ISM predicted the induced distortions with greater accuracy. The surface deviations for the shell model with the analytical thermal solution are shown in Figures 5d, 6d and 7d. It can be seen that the shrinkage is greater than the shell model using ISM. The two shell models were not able to capture the buckling effect in comparison to the solid elements on the side of the manifold. This indicates a possible limitation of the shell elements.
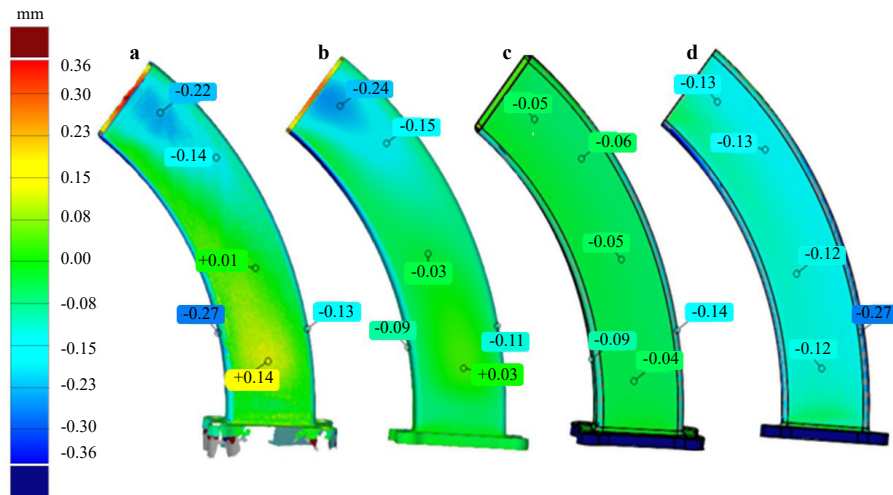
Figure 5. Surface deviation on the side: a) Manufactured manifold; b) Solid model-ISM; c) Shell-ISM; d) Shell-Analytical thermal model

Although overall the solid model shows better results than the shell models, it is notable that the shell model using ISM is able to predict the distortion in specific areas. However, there may be other geometries where the ISM with shell elements may be also feasible. In addition, it may be applicable to use a combination of both solid and shell elements for complex geometries (e.g., support structures that can be modelled with shell elements). The use of shell elements could be combined with beam elements to represent lattice structures enabling fast computing. However, this needs to be further researched.
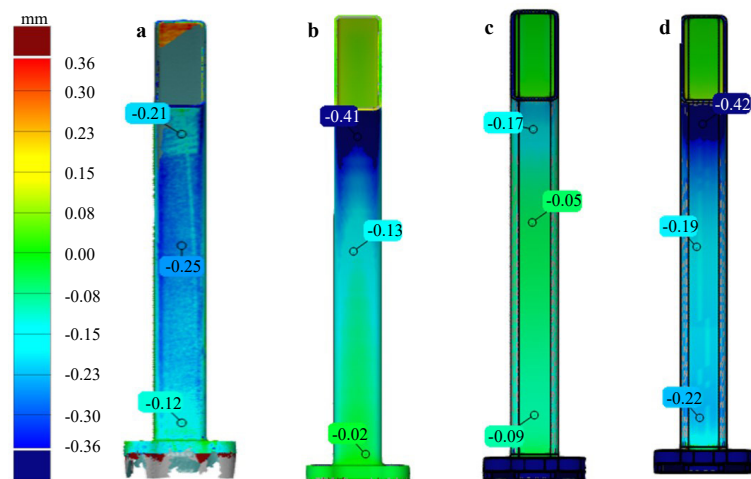
Figure 6. Surface deviations in the inner edge: a) Manufactured manifold; b) Solid model-ISM; c) Shell-ISM; d) Shell-Analytical thermal model
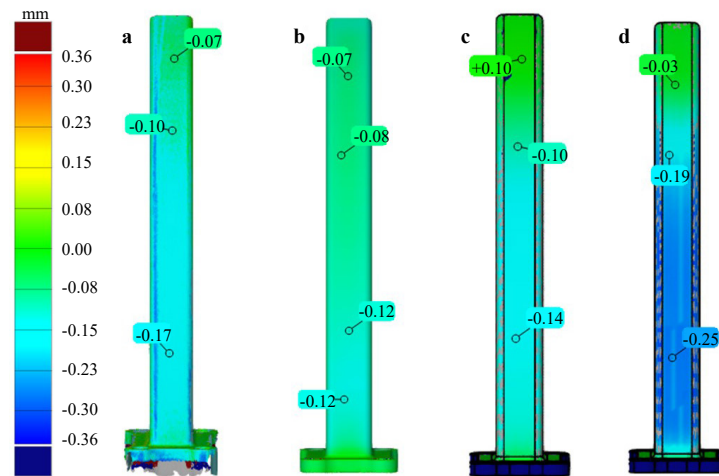
Figure 7. Surface deviations in the outer edge: a) Manufactured manifold; b) Solid model-ISM; c) Shell-ISM; d) Shell-Analytical thermal model

4. Conclusion

The following conclusions were derived from this research work:

i.   Shell elements can be successfully used for the simulation of the build process in LPBF with a reasonable degree of accuracy in the inner and the outer sides of a manifold component when combined with the ISM.

ii. One of the limitations of the shell elements is the inability to capture the buckling effect induced during the fabrication of a thin-walled manifold using LPBF.

iii. The ISM combined with solid elements was able to predict the buckling behaviour but the distortions in the inner side of the manifold were overpredicted.

iv. The shell model with the analytical thermal model predicted greater shrinkage and delivered less accurate predictions of distortion.

v.   The shell model using the ISM computed 2.4 times faster than the model using solid elements.

vi. The distortion predictions of the three models showed some similarities to the actual measured distortions, but none of the three models accurately predicted the distortion in all the areas of the manifold geometry. This indicates that further research is required to handle the distortion in thin manifold geometries.

vii. The shell element can be used for representing support structures where the exact prediction of distortion is less important, but the reduction of computational time might be sought.

References

[1] Hernández-Pérez JC, Osorio-Gómez G, Mejía-Gutiérrez R. From functional prototypes to industrial products. *International Journal on Interactive Design and Manufacturing*. 2017; 11: 155-171. Available from: doi. org/10.1007/s12008-015-0260-9.

[2] Chen Q, Guillemot G, Gandin CA, Bellet M. Finite Element Modeling of Ceramic Deposition by LBM(SLM) Additive Manufacturing. In: Meboldt M, Klahn C. (eds.) *Industrializing Additive Manufacturing - Proceedings of Additive Manufacturing in Products and Applications*. Springer; 2018. p.49-58.

[3] Mercelis P, Kruth J. Residual stresses in selective laser sintering and selective laser melting. *Rapid Prototyping Journal*. 2006; 12(5): 254-265. Available from: doi.org/10.1108/13552540610707013.

[4]   Acevedo R, Sedlak P, Kolman R, Fredel M. Residual stress analysis of additive manufacturing of metallic parts using ultrasonic waves: State of the art review. *Journal of Materials Research and Technology*. 2020; 9(4): 9457-9477. Available from: doi.org/10.1016/j.jmrt.2020.05.092.

[5]   Yaghi A, Afazov S, Villa M. Maturity Assessment of Laser Powder Bed Fusion Process Chain Modelling and Simulation. *Digital Manufacturing Technology*. 2021; 1 (1): 34-45. Available from: doi.org/10.37256/dmt.112021822.

[6]   Bayat M, Dong W, Thorborg J, To A, Hattel. A review of multi-scale and multi- physics simulations of metal additive manufacturing processes with focus on modeling strategies. *Additive Manufacturing*. 2021; 47: 102278. Available from: doi.org/10.1016/j.addma.2021.102278.

[7]   Peter N, Pitts Z, Thompson S, Saharan A. Benchmarking build simulation software for laser powder bed fusion of metals. *Additive Manufacturing*. 2020; 36: 101531. Available from: doi.org/10.1016/j.addma.2020.101531.

[8]   Bugatti M, Semeraro Q. Limitations of the inherent strain method in simulating powder bed fusion processes. *Additive Manufacturing*. 2018; 23: 329-346. Available from: doi.org/10.1016/j.addma.2018.05.041.

[9]   Lindgren LE. Thermomechanical and Microstructural Simulations. In: *Computational Welding Mechanics: Woodhead Publishing Series in Welding and Other Joining Technologies*. Elsevier; 2007. p.31-46. Available from: doi.org/10.1533/9781845693558.31.

[10]   Gysin H, Gantenbein R. Simulation of Additive Manufacturing Processes for Metals: Amazing Experiences. In: *NAFEMS World Congress 2019*. Available from: https://www.simufact.com/files/Medien/_6NewsundEvents/Articles/english/Simufact-A-Copyright-NAFEMS-Simulation-of-Additive-Manufacturing-Processes-for-Metals-Amazing-Experiences.pdf [Accessed 10th May 2022].

[11]   Liang W, Murakawa H. Predicting Welding Distortion in a Panel Structure with Longitudinal Stiffeners Using Inherent Deformations Obtained by Inverse Analysis Method. *The Scientific World Journal*. 2014; 2014: 601417. Available from: doi.org/10.1155/2014/601417.

[12]   Afazov S, Denmark W, Toralles B, Holloway A, Yaghi A. Distortion prediction and compensation in laser selective melting. *Additive Manufacturing*. 2017; 17: 15-22. Available from: doi.org/10.1016/j.addma.2017.07.005.

[13]   Afazov S, Roberts A, Wright L, Jadhav P, Holloway A, Basoalto H, et al. Metal powder bed fusion process chains: an overview of modelling techniques. *Progress in Additive Manufacturing*. 2022; 7: 289-314. Available from: doi.org/10.1007/s40964- 021-00230-1.

[14]   Deng D, Murakawa H, Liang W. Numerical simulation of welding distortion in large structures. *Computer Methods in Applied Mechanics and Engineering*. 2007; 196(45-48): 4613-4627. Available from: doi.org/10.1016/j.cma.2007.05.023.

[15]   Afazov S, Rahman H, Serjouei A. Investigation of the right-time distortion compensation approach in laser power bed fusion of a thin manifold structure made of Inconel 718. *Journal of Manufacturing Processes*. 2021; 69: 621-629. Available from: doi.org/10.1016/j.jmapro.2021.08.016.

[16]   Liang X, Chen Q, Cheng L, Yang Q, To A. A Modified Inherent Strain Method for Fast Prediction of Residual Deformation in Additive Manufacturing of Metal Parts. In: *Solid Freeform Fabrication 2017: Proceedings of the 28th Annual International Solid Freeform Fabrication Symposium - An Additive Manufacturing Conference*. 2017. p.2539-2545. Available from: http://utw10945.utweb.utexas.edu/sites/default/files/2017/Manuscripts/AModifiedInherentStrainMethodforFastPredict.pdf [Accessed 10th May 2022].